



Ionic liquid-functionalized amphiphilic Janus nanosheets afford highly accessible interface for asymmetric catalysis in water



Chaoping Li, Su Liu, Yibing Pi, Jingwen Feng, Zewei Liu, Shiye Li, Rong Tan*

National & Local Joint Engineering Laboratory for New Petro-chemical Materials and Fine Utilization of Resources, Key Laboratory of Chemical Biology and Traditional Chinese Medicine Research (Ministry of Education), College of Chemistry & Chemical Engineering, Hunan Normal University, No. 36, South Lushan Road, Changsha, Hunan 410081, PR China

ARTICLE INFO

Article history:

Received 20 October 2020

Revised 17 January 2021

Accepted 18 January 2021

Available online 28 January 2021

Keywords:

Aqueous asymmetric catalysis

Ionic liquid

Janus mesosilica nanosheets

Pickering emulsion

Asymmetric sulfoxidation

ABSTRACT

High oil/water interfacial area together with accessible interfaces for reagents is the key to achieving efficient asymmetric catalysis in water. Herein, by taking advantage of the excellent interfacial activity of Janus nanosheets (JNS), as well as the unique compatibility of imidazolium ionic liquid (IL), we developed a series of IL-functionalized amphiphilic Janus mesosilica nanosheets which afford highly accessible reaction interfaces for highly enantioselective sulfoxidation in water. The JNS-typed chiral salen Ti^{IV} catalysts were prepared by selectively decorating hydrophobic chiral salen Ti^{IV} complex on one side of Janus mesosilica nanosheets through the imidazolium-based IL linker. Benefiting from the two-dimensional porous Janus structure, as well as the compatible IL linker, the IL-tagged JNS catalysts afforded high oil/water interfacial areas and highly accessible reaction interface for sulfides and H₂O₂, significantly accelerating asymmetric sulfoxidation in water using H₂O₂ as an oxidant. In addition, they can be facilely recovered for stable reuse by simple centrifugation.

© 2021 Elsevier Inc. All rights reserved.

1. Introduction

Asymmetric catalysis in water is of great interest in chemical industry not only due to the green and sustainable process, but also because water often exerts a positive effect on chemical reactivity and selectivity [1,2]. However, they often suffered from low reaction rate because of limited interfacial area and huge mass transfer resistance. Surfactant-like catalysts can enhance the mass transfer between oil/water phases through emulsification, but are not favorable for industrial use due to the troublesome separation and reusability [3]. Janus colloids which combine the unique features of both traditional surfactant (e.g., amphiphilicity) and inorganic materials (e.g., heterogeneous properties) have emerged as the alternative interfacial catalysts for aqueous catalysis [4–6]. Compared with traditional surfactants, the Janus colloids offer a higher interfacial activity, forming more stable Pickering emulsion with maximal oil/water interfacial area [7–9]. Moreover, the interfacial reaction relying on solid particles allows for facile separation and recycling of catalysts. Organic products should be in situ separated from the aqueous systems due to the difference in water–oil solubility, which avoids the complicated separation and purification process [10].

Amphiphilic JNS with asymmetric wettability on opposing sides have recently received increasing concerns in the Pickering interfacial catalysis, due to their excellent interfacial activity and highly anisotropic shape [11–13]. Their excellent interfacial activity enables them to be steadily adhered on the oil/water interface, giving stable Pickering emulsion with maximal oil/water interfacial area. Highly anisotropic shape greatly restricted their rotation of the JNS at the oil/water interface, thus making the emulsion more stable [14,15]. More interestingly, two-dimensional sheet-shaped materials assembled at oil/water interfaces provide a short diffusion distance between oil and water, which is critical for the mass transfer on the interfaces [16–18]. However, with a strong interfacial adhesion, JNS themselves may serve as a physical barrier between the oil/water interfaces, making the reaction interfaces inaccessible. Yang *et al.* synthesized mesoporous JNS and loaded ultrafine Pd nanoparticles in the mesochannels. The abundant mesochannels present on JNS provided efficient passageway for reagents, ensuring accessibility of the catalytically active interface for nitroarene hydrogenation in water [19]. Nonetheless, this strategy only allows ultrafine catalytic species within the pores. If bulk chiral metal complex is involved, it inevitably obstructs the diffusion of reactants. More importantly, the nanosized pores may restrain the conformational freedom of embedded chiral catalytic species, which is undesirable for asymmetric catalysis [20,21]. If bulk catalytic active species is selectively decorated on one side

* Corresponding author.

E-mail address: yiyangtanrong@126.com (R. Tan).

of mesoporous JNS, leaving the channels free, it would be possible to achieve highly accessible reaction interfaces with excellent asymmetric induction. However, the JNS-based chiral catalysts have rarely been reported for aqueous asymmetric catalysis to date.

Bulk chiral metallosalen complexes are privileged catalysts, as demonstrated by their successful application in a wide variety of challenging field ranging from materials chemistry to organic synthesis [22,23]. Herein, we selectively grafted hydrophobic chiral salen Ti^{IV} complex on one side surface of hydrophilic mesosilica nanosheet, to develop the amphiphilic JNS-type Ti(salen) catalyst for asymmetric sulfoxidation in water. An imidazolium IL was introduced as a flexible linker between the bulk Ti(salen) units and mesosilica surface. Apart from ensuring the necessary conformation freedom of Ti(salen) groups, the IL modifier with unique compatibility will fine-tune the surface properties of mesosilica and transfer the ILs' properties to material, which thus makes the reaction interface more accessible for reactants [24,25]. Benefiting from the two-dimensional porous Janus structure, as well as the unique IL linker, our JNS-type Ti(salen) catalysts not only displayed an excellent interfacial activity but also provide a highly accessible reaction interface for organic sulfides and aqueous H₂O₂ in asymmetric sulfoxidation in water. Extremely high activity (conversion of 92–98%), chemo- (95–99%) and enantioselectivity (88–99%) were achieved for a wide range of sulfides, while traditional chiral salen Ti^{IV} complex was far less efficient. Furthermore, the catalysts can be quantitatively recovered from the aqueous system by centrifugation for steady reuse. Such IL-functionalized JNS materials combine the benefits of chiral phase-transfer and heterogeneous catalyst, and avoid the tedious procedures of separation, which is a benefit for energy-saving and industrial applications.

2. Experimental

2.1. Materials and reagents

Poly(vinyl pyrrolidone) (PVP, $M_w = 40000$), 2,2-azobis(2-methyl propionitrile) (AIBN), *N*-[3-(triethoxysilyl)propyl]-4,5-dihydroimidazole and 2,2'-azobis[2-methylpropionamide] dihydrochloride (AIBA) were obtained by Macklin. 3-Aminopropyltriethoxysilane (APTES) and lysine were obtained from Aladdin. Tetraethoxysilane (TEOS), phenyl methyl sulphide, phenyl ethyl sulphide and chloroauric acid was obtained from Aldrich. 4-Methoxyphenyl methyl sulfide, 2-methoxyphenyl methyl sulfide, and 4-bromophenyl methyl sulfide were obtained from J&K. 2-*tert*-Butyl phenol was purchased from Alfa Aesar. Other commercially available chemicals and solvents were obtained from local suppliers by standard procedure without further purification.

Phenyl *n*-butyl sulfide and phenyl *n*-hexyl sulfide were synthesized according to Ref. [26]. Alkoxysilane reagents of (C₂H₅O)₃Si-IL/Ti(salen) and (C₂H₅O)₃Si-Ti(salen) (Chart 1) were synthesized as described procedure in Ref. [27]. [(*R,R'*)-[*N,N'*-(3,5-di-*tert*-butylsalicylidene)-1,2-cyclohexanediaminato]titanium(IV) diisopropyl (denoted as neat complex, Chart 2) was synthesized

according to the described procedure in Ref. [28]. Polystyrene (PS) microsphere was synthesized according to the procedure in Ref. [29]. PS@mSiO₂ where porous silica layer was coated on PS microsphere was synthesized according to the procedure in Ref. [19]. PS@SiO₂ where non-porous silica layer was coated on PS microsphere was synthesized according to the procedure in Ref. [30].

2.2. Analytical methods

Fourier-transform infrared spectroscopy (FT-IR) spectra were recorded on AVATAR 370 Thermo Nicolet spectrophotometer using potassium bromide pellets in the range of 400–4000 cm⁻¹. Nuclear magnetic resonance (NMR) spectra were represented by a BRUKER AVANCE-500 spectrometer. Titanium contents of samples were determined by inductively coupled optical emission spectra (ICP-OES) on an Agilent 5110. Transmission electron microscopy (TEM) micrographs were obtained on a Microscope Tecnai F20 at an accelerating voltage of 200 kV. Scanning electron microscopy (SEM) was performed with a HITACHI S-4800 apparatus operated at an accelerating voltage of 15 kV. N₂ adsorption–desorption isotherms were obtained on TriStar 3000-Micromeritics. The composites were degassed at 120 °C for 6 h before measuring the isotherms. Water contact angles (WCA) of the samples were measured by the static sessile drop method on a Theon TX500TM (Kono Corp.) instrument. Samples were directly compressed without the aid of binder. A drop of deionized water was then placed on it and imaged by camera. Microscope images of sulfide-in-water emulsions were obtained on BX53M (Olympus Corp.). The conversion and chemoselectivity to chiral sulfoxides were analyzed by a 6890N gas chromatograph (Agilent Co.) using equipped with a capillary column (HP19091G-B213, 30 m × 0.32 mm × 0.25 μm) and a FID detector. Enantioselectivity (*E_e* value) of chiral sulfoxides was determined by HPLC analysis using Daicel Chiralpak AD column.

2.3. Preparation of the IL-functionalized JNS catalysts (denoted as JNS-IL/Ti(salen)_x)

JNS-IL/Ti(salen)_x were prepared via simply crushing hollow mesosilica microspheres with two distinct surfaces, as shown in Scheme 1.

Synthesis of PS@mSiO₂. The PS@mSiO₂ where a silica layer with perpendicular mesochannels was coated on the PS microspheres was synthesized via a sol-gel method [19]. PS microsphere (1.92 g) and cetyltrimethyl ammonium bromide (CTAB, 2.6 mmol, 0.96 g) were added into mixed solvent of ethanol (120 mL) and water (100 mL). After stirring for 30 min, TEOS (2.7 mmol, 0.6 mL) was quickly added. The obtained mixture was stirred at room temperature for 6 h, and then kept undisturbed at 80 °C overnight. After being centrifuged, PS@mSiO₂ was washed with deionized water, and subsequently dried under vacuum at room temperature for 12 h.

Synthesis of JNS-IL/Ti(salen)_x. PS@mSiO₂ (1.0 g) was dispersed in ethanol (50 mL) by ultrasound. Alkoxysilane reagent of

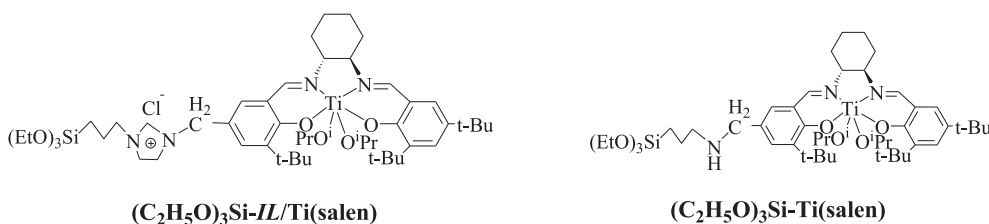


Chart 1. The structures of (C₂H₅O)₃Si-IL/Ti(salen) and (C₂H₅O)₃Si-Ti(salen).

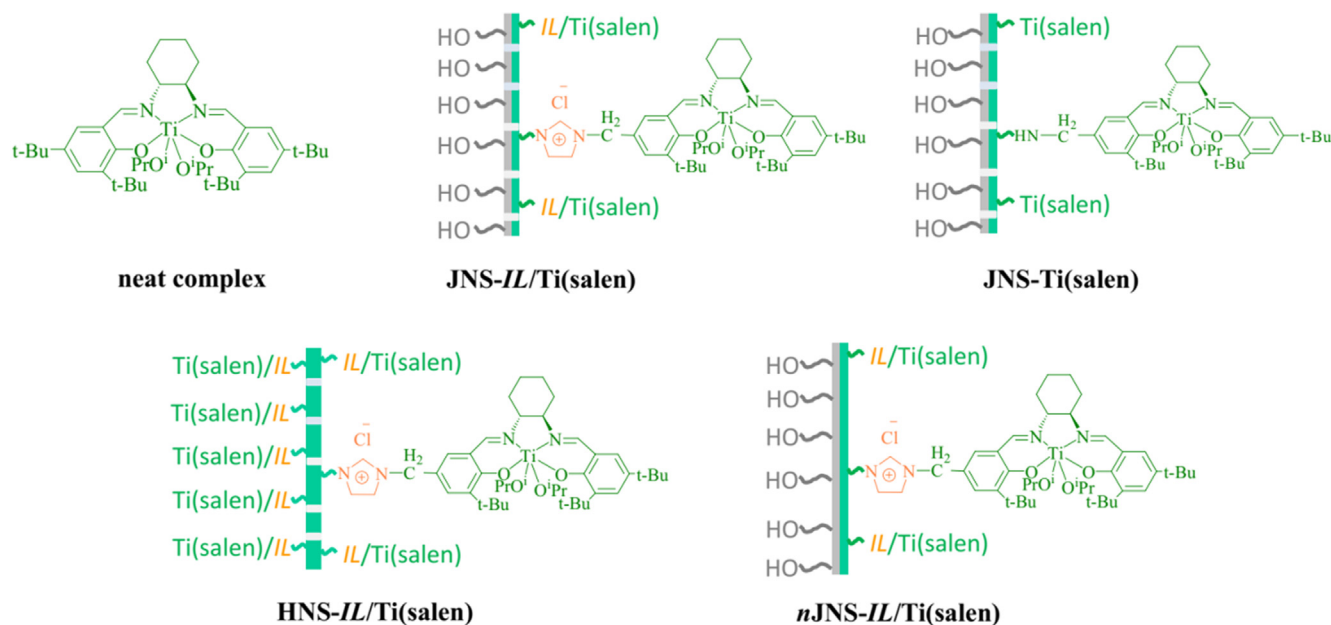
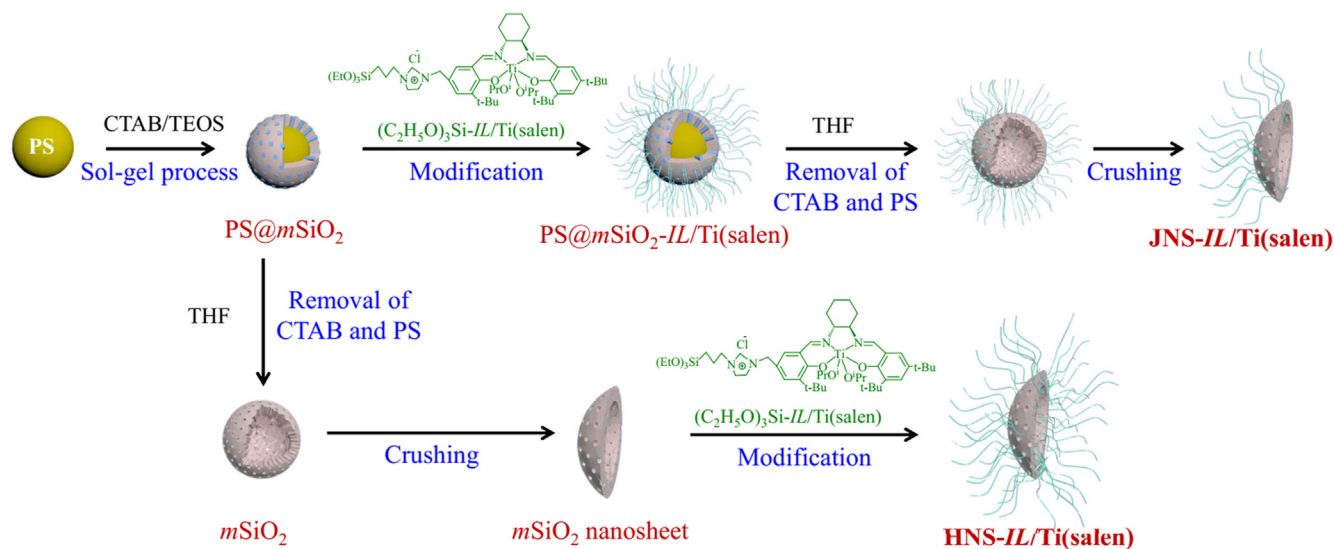


Chart 2. Their representative structures of neat complex, $\text{JNS-IL/Ti(salen)}_x$, JNS-Ti(salen) , HNS-IL/Ti(salen) , and $n\text{JNS-IL/Ti(salen)}$.



Scheme 1. Synthesis of $\text{JNS-IL/Ti(salen)}_x$ ($x = 0.38, 0.48, 0.60$) and HNS-IL/Ti(salen) .

$(\text{C}_2\text{H}_5\text{O})_3\text{Si-IL-Ti(salen)}$ (0.4 mmol for $\text{JNS-IL/Ti(salen)}_{0.38}$, 0.6 mmol for $\text{JNS-IL/Ti(salen)}_{0.48}$, and 1.0 mmol for $\text{JNS-IL/Ti(salen)}_{0.60}$) was then added to the dispersion, and the resulting mixture was refluxed at 80 °C for 12 h. After centrifugation, the as-made $\text{PS@mSiO}_2\text{-IL/Ti(salen)}$ sample was treated with THF (75 mL) at 25 °C for 12 h, to remove templates of CTAB and PS completely. IL/Ti(salen) -coated hollow mesosilica microspheres were subsequently collected by centrifugation (10000 rpm, 10 min), washed with ethanol for several times, and then dried under vacuum. Crushing the IL/Ti(salen) -coated hollow mesosilica microspheres gave Janus silica nanosheets of $\text{JNS-IL/Ti(salen)}_x$ as light yellow powder (where x represents the titanium content in samples, $x = 0.38, 0.48$, and $0.60 \text{ mmol}\cdot\text{g}^{-1}$). IL/Ti(salen) and hydroxyl groups are distinctly located on the corresponding sides of the mesosilica nanosheets, as shown in Chart 2. $\text{JNS-IL/Ti(salen)}_{0.38}$: FT-IR: $\gamma_{\text{max}}/\text{cm}^{-1}$: 3451, 2950, 2927, 2868, 1715, 1655, 1632, 1551, 1466, 1384, 1315, 1191, 1090, 807, 693, 618, 568, 466. Titanium content:

$0.38 \text{ mmol}\cdot\text{g}^{-1}$. $\text{JNS-IL/Ti(salen)}_{0.48}$: FT-IR: $\gamma_{\text{max}}/\text{cm}^{-1}$: 3451, 2954, 2924, 2871, 1719, 1652, 1631, 1551, 1466, 1384, 1315, 1187, 1089, 807, 692, 622, 569, 464. Titanium content: $0.48 \text{ mmol}\cdot\text{g}^{-1}$. $\text{JNS-IL/Ti(salen)}_{0.60}$: FT-IR: $\gamma_{\text{max}}/\text{cm}^{-1}$: 3451, 2951, 2924, 2924, 2856, 1651, 1551, 1466, 1384, 1315, 1187, 1090, 808, 692, 622, 564, 470. Titanium content: $0.60 \text{ mmol}\cdot\text{g}^{-1}$.

2.4. Preparation of the IL-free JNS counterpart of JNS-Ti(salen)

An IL-free counterpart of JNS-Ti(salen) was also prepared according to a similar preparation procedure to that of $\text{JNS-IL/Ti(salen)}_x$. During the procedure, the organosiloxane of $(\text{C}_2\text{H}_5\text{O})_3\text{Si-Ti(salen)}$ was used instead of the $(\text{C}_2\text{H}_5\text{O})_3\text{Si-IL-Ti(salen)}$ to modify the external surface of PS@mSiO_2 . After complete removal of CTAB and PS templates, the obtained Ti(salen) -coated hollow mesosilica microspheres were crushed into JNS-Ti(salen) , where Ti(salen) was directly decorated on one side surface of mesosilica

nanosheets through an alkyl linker. The representative structure of **JNS-Ti(salen)** was shown in [Chart 2](#). FT-IR: $\gamma_{\max}/\text{cm}^{-1}$ 3451, 3081, 3061, 3026, 2926, 1623, 1439, 1452, 1384, 1313, 1186, 1083, 813, 757, 697, 568, 466. Titanium content: 0.48 mmol·g⁻¹.

2.5. Preparation of homogeneous counterpart of **HNS-IL/Ti(salen)**

To investigate the “Janus effect” of **JNS-IL/Ti(salen)_x**, a homogeneous counterpart of **HNS-IL/Ti(salen)** ([Chart 2](#)) where *IL*/Ti(salen) groups were uniformly dispersed on both sides of the mesosilica nanosheets was prepared as a control catalyst, as shown in [Scheme 1](#). PS@mSiO₂ (1.0 g) was treated with THF (75 mL) at 25 °C for 12 h to remove CTAB and PS completely. The obtained hollow silica microspheres were crushed into silica nanosheets, and then modified with (C₂H₅O)₃Si-*IL*/Ti(salen) (0.6 mmol, 0.59 g) in toluene (50 mL) at 80 °C for 12 h. Removal of the unreacted (C₂H₅O)₃Si-*IL*-Ti(salen) afforded the **HNS-IL/Ti(salen)** as light yellow powder. FT-IR (KBr): $\gamma_{\max}/\text{cm}^{-1}$: 3451, 2953, 2924, 2875, 1718, 1656, 1632, 1551, 1466, 1385, 1319, 1090, 964, 808, 692, 619, 568, 466. Titanium content: 0.48 mmol·g⁻¹.

2.6. Preparation of the nonporous JNS counterpart of **nJNS-IL/Ti(salen)**

Furthermore, a nonporous counterpart of **nJNS-IL/Ti(salen)** ([Chart 2](#)) was also prepared as the control catalyst to investigate the “passageway effect” of mesochannels. The preparation procedure was similar to that of **JNS-IL/Ti(salen)**. PS@SiO₂ where nonporous silica layer was coated on PS microsphere [30] was used instead of PS@mSiO₂ during the procedure. The abundant surface hydroxyl groups (—OH) present on PS@SiO₂ were readily reacted with the alkoxy silane reagent of (C₂H₅O)₃Si-*IL*/Ti(salen) through silylation, giving the *IL*/Ti(salen)-coated PS@SiO₂ microspheres. After removal of PS template, the obtained hollow spheres were crushed into the nonporous **nJNS-IL/Ti(salen)**. FT-IR (KBr): $\gamma_{\max}/\text{cm}^{-1}$: 3451, 2952, 2926 2870, 1715, 1651, 1628, 1551, 1466, 1384, 1315, 1187, 1090, 807, 692, 623, 569, 466. Titanium content: 0.49 mmol·g⁻¹.

2.7. General procedure for asymmetric sulfoxidation in water

The selected catalyst (0.9 mol% of substrate, based on titanium content) was stirred with sulfides (0.5 mmol) in deionized water (1 mL) at 25 °C. H₂O₂ (30 wt%, 0.6 mmol) was then added dropwise over 15 min. The resulting mixture was stirred at 25 °C. Reaction progress was monitored by TLC. After the reaction, the catalytic systems were subjected to demulsification through high speed centrifugation (18000 r/min) for 15 min. Catalyst was completely precipitated from the aqueous system. Recovered catalyst was washed with ethanol, dried in a vacuum, and finally recharged with fresh substrate and oxidant for the next catalytic cycle. Organic product in aqueous phase was extracted with ethyl acetate (3 × 4 mL). Notably, the extraction process should be excluded in large-scale industrial processes, in which the oily product phase can be directly separated from water after demulsification. Combined organic layer was dried over anhydrous sodium sulfate, and then purified by chromatography on silica gel (petroleum ether/ethyl acetate, 5: 1). The depurated chiral sulfoxides have been identified by ¹H NMR spectra. Ee values of the products were determined by HPLC analysis using the Daicel chiralpak AD columns. Detailed NMR and HPLC analyses for the sulfoxides are available in ESI.

3. Results and discussion

3.1. Preparation of catalysts

Pickering emulsions offers an efficient platform for the asymmetric catalysis in water, because it provides a high interfacial reaction area per unit volume, improves the compatibility between hydrophilic and hydrophobic reagents, and facilitates the mass transfer [31]. Amphiphilic JNS with mesoporous structure are very suitable as Pickering interfacial catalysts for the aqueous catalysis. On one hand, the two-dimensional materials with highly anisotropic shapes and surface chemistry can steadily adhere to immiscible oil/water interface, forming stable Pickering emulsions and thus providing larger interfacial areas. On the other hand, the abundant mesoporous channels present at the interface benefit the contact between the reactants inside and outside the droplets [27,32,33]. With those points in mind, we decided to selectively graft chiral salen Ti^{IV} complex on one side of mesosilica nanosheet to develop the amphiphilic JNS-type chiral salen Ti^{IV} catalyst for efficient asymmetric sulfoxidations in water. Imidazolium-based *IL* was used as a flexible linker between chiral salen Ti^{IV} complex and mesosilica surface. Apart from ensuring conformational freedom of Ti(salen), the *IL* linker also stabilizes the formed metallosalen active intermediates, thereby further enhancing the catalytic efficiency of the chiral metallosalen catalyst [34]. More importantly, such an *IL* moiety with unique solvent power may transfer the compatible properties to JNS material, which is expected to further improve the accessibility of catalytically active interface [35].

The preparation of *IL*-functionalized amphiphilic JNS catalysts was shown in [Scheme 1](#). First, silica shell with perpendicular mesochannels was coated on PS microspheres *via* a sol-gel method by using TEOS as a silica source and CTAB as a soft template. The obtained PS@mSiO₂ was surface-modified with organosiloxane of (C₂H₅O)₃Si-*IL*/Ti(salen) through silylation. Since CTAB still occupied the mesochannels, the bulk organosiloxane are difficult to diffuse into mesochannels and internal surface of the mesosilica shell. As a result, most of Ti(salen) groups were grafted on the external surface of PS@mSiO₂ through an *IL* linker. The Ti(salen) loading could be fine tuned by changing the organosiloxane concentration. Removal of the CTAB and PS affords the Janus hollow mesosilica sphere which is covered by *IL*/Ti(salen) group. The hollow microspheres were finally crushed by a simple grind, giving *IL*-functionalized amphiphilic JNS catalysts of **JNS-IL/Ti(salen)_x**. Hydrophobic *IL*/Ti(salen) and hydrophilic Si-OH groups are distinctly terminated onto the corresponding sides of **JNS-IL/Ti(salen)_x**. Their representative structure is shown in [Chart 2](#).

3.2. Characterization of samples

3.2.1. FT-IR

The successful decoration of *IL*/Ti(salen) moiety on mesosilica nanosheet was verified by FT-IR. [Fig. 1](#) shows the FT-IR spectra of typical **JNS-IL/Ti(salen)_{0.48}**, **JNS-Ti(salen)**, as well as pristine mesosilica nanosheet and neat complex for comparison. Clearly, pristine mesosilica nanosheet shows distinct characteristic bands at 3451, 1090 and 807 cm⁻¹, which are assigned to the skeletal vibrations of O—H, Si—O—Si and Si—OH groups, respectively ([Fig. 1a](#)) [28]. Upon silylation with (C₂H₅O)₃Si-*IL*-Ti(salen), the characteristic bands of O—H and Si—OH groups significantly weaken, although they are also present in the FT-IR spectrum of typical **JNS-IL/Ti(salen)_{0.48}** ([Fig. 1b](#)). It provided convincing evidence that partial surface hydroxyl groups on mesosilica nanosheet have participated in silylation with the *IL*/Ti(salen)-containing organosiloxane. Indeed, the FT-IR spectrum of **JNS-IL/Ti(salen)_{0.48}** exhibited the stretching vibrations of —CH₂— (in the

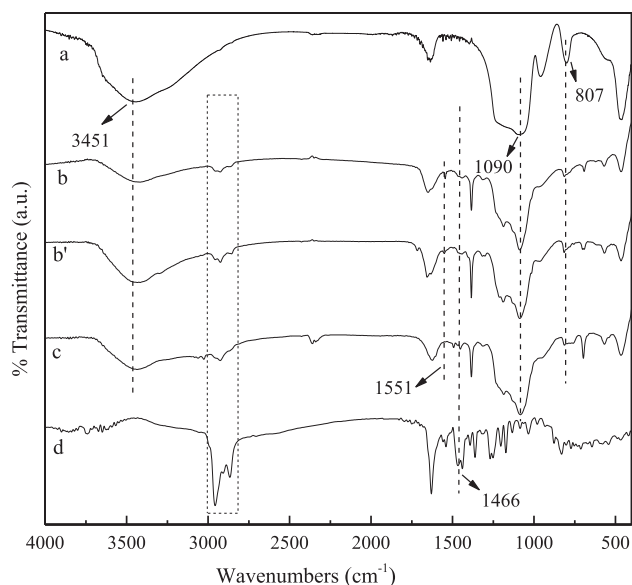


Fig. 1. FT-IR spectra of pristine mesosilica nanosheet (a), typical **JNS-IL/Ti(salen)_{0.48}** (b), the recovered **JNS-IL/Ti(salen)_{0.48}** after the 7th reuse (b'), **JNS-Ti(salen)** (c), and neat complex (d).

range of 2821–3000 cm^{-1}) and Ph-H (at 1466 cm^{-1}) in **Ti(salen)** and imidazole ring in **IL** moiety (at 1551 cm^{-1}) [28]. Notably, the CTAB molecules still occupied the mesochannels during the silylation process, bulk organosilane of $(\text{C}_2\text{H}_5\text{O})_3\text{Si-IL-Ti(salen)}$ is difficult to diffuse into the inner surface of mesosilica shell. We can thus envision that most chiral **salen Ti^{IV}** complexes are just located on external surface of the mesosilica shell, leaving the inner surface free. The region-selective modification not only makes the **JNS-IL/Ti(salen)_x** catalytically active, but also endows them unique Janus structure and excellent interfacial activity, which are crucial in Pickering interfacial catalysis. The **IL-free** counterpart of **JNS-Ti(salen)** exhibited similar FT-IR spectrum to **JNS-IL/Ti(salen)_{0.48}** (Fig. 1c vs. 1b), except for the absence of characteristic stretching vibrations of the imidazole ring (near 1551 cm^{-1}). The difference is related to the inexistence of imidazolium-based **IL** linker in the framework of **JNS-Ti(salen)**. Actually, compared with **JNS-Ti(salen)**, a significant feature observed for **JNS-IL/Ti(salen)_{0.48}** is the presence of an imidazolium-based **IL** linker that positively affects catalytic performance in the aqueous catalysis. Notably, all active species of **Ti(salen)** are intact during the grafting as its characteristic bands in silica-supported samples are identical to those in neat complex (Fig. 1b and 1c vs. 1d).

3.2.2. SEM and TEM

SEM and TEM images provide information for the morphology of as-prepared **JNS-IL/Ti(salen)_x**. As shown in Fig. 2, spherical particles with an average diameter of ca. 2.8 μm are observed on the SEM image of **PS@mSiO₂** (Fig. 2a). Surface modification and followed template removal give Janus hollow silica microsphere with a shell of 78 nm in thickness (Fig. 2b). After being milled, almost all the Janus hollow microspheres have been crushed into Janus mesosilica nanosheets, as shown in the SEM image (Fig. 2c). Cross-sectional SEM image reveals that the thickness of nanosheet is approximately 78 nm (the inset in Fig. 2c), which is consistent with the shell thickness of hollow microsphere. Furthermore, abundant nanopores (3–5 nm) are found to be dispersed throughout on the resultant **JNS-IL/Ti(salen)_x** ($x = 0.38, 0.48, \text{ and } 0.60 \text{ mmol}\cdot\text{g}^{-1}$) (see TEM images of Fig. 2d and Fig. S1 in ESI), which are generated from the removal of CTAB species occupying the frameworks of silica shell. HRTEM image of **JNS-IL/Ti(salen)_{0.48}**

distinctly exhibits a perpendicular pattern of the mesochannels with the size of about 3.8 nm (the inset in Fig. 1d). Such a mesoporous structures should provide enough passageway to ensure mass accessibility of the interfacial catalysis. **JNS-Ti(salen)** and **HNS-IL/Ti(salen)** display similar 2D sheet-like mesoporous morphology (Fig. 2e and 2f vs. 2c), while, any nanopores cannot be observed in the nanosheets of **nJNS-IL/Ti(salen)** (Fig. 2g), confirming the nonporous morphology of **nJNS-IL/Ti(salen)**. To prove Janus character of **JNS-IL/Ti(salen)_x**, Pd NPs were used to label JNS instead of **IL/Ti(salen)** via electrostatic interaction (detailed procedure is available in section S1 of ESI). Clearly, most of Pd NPs are selectively labeled on one side of the mesosilica nanosheet, leaving the other side smooth (Fig. 2h). This region-selective modification is agree with the distinct compartmentalization of hydrophilic **Si-OH** and hydrophobic **IL/Ti(salen)** groups onto both sides of **JNS-IL/Ti(salen)_x**, respectively.

3.2.3. Nitrogen adsorption–desorption

Porous structure of **JNS-IL/Ti(salen)_x** ($x = 0.38, 0.48, 0.60$) was further investigated by nitrogen adsorption–desorption, as shown in Fig. 3. Different from **nJNS-IL/Ti(salen)** which is nonporous (Fig. 3A), typical **JNS-IL/Ti(salen)_{0.48}** exhibit a hysteresis loop at $P/P_0 > 0.45$ in its sorption isotherm, featuring mesoporous material (Fig. 3B) [36]. The pore diameter is centered at 3.81 nm in pore size distributions curve, which is consistent with the size observed in TEM image. Notably, pore size of **JNS-IL/Ti(salen)_{0.48}** (3.81 nm) is approximate to that of pristine mesosilica nanosheet (3.83 nm) (Fig. 3B vs. 3C). It is the convincing evidence that **IL/Ti(salen)** groups are grafted just on mesosilica surface, rather than being entrapped into the channel. For this reason, it is not surprised that the pore size of **JNS-IL/Ti(salen)_x** remains almost constant as the **Ti(salen)** loading varied from 0.38 to 0.60 $\text{mmol}\cdot\text{g}^{-1}$ (Fig. S2 in ESI). Furthermore, homogeneous **HNS-IL/Ti(salen)** exhibit similar textural parameters to **JNS-IL/Ti(salen)_x**, due to the similar surface modification (Fig. 3D). The unhindered channels may ensure diffusion and mass accessibility of the interfacial catalysis, giving rise to prominent catalytic activity.

3.2.4. Surface wettability determination

WCA was used to evaluate the surface wettability of **JNS-IL/Ti(salen)_x**, which is crucial in dictating the type of formed Pickering emulsions. Pristine **mSiO₂** sheet exhibits a WCA of 26°, suggesting its highly hydrophilic surface (Fig. 4a). The WCA value increases upon the hydrophobic modification of **IL/Ti(salen)** on mesosilica surface, and can be fine tuned by tailoring the **IL/Ti(salen)** loading. When the content of **IL/Ti(salen)** increased from 0.38 to 0.60 $\text{mmol}\cdot\text{g}^{-1}$, WAC of **IL-functionalized JNS** is controlled from 60 to 82°, accordingly (Fig. 4b–d). These trends agree well with the tendency of its hydrophobic/hydrophilic balance. With similar titanium loading, **HNS-IL/Ti(salen)** and **nJNS-IL/Ti(salen)** exhibits the WCA values close to **JNS-IL/Ti(salen)_{0.48}** (76°) (Fig. 4e and 4g vs. 4c), while, **IL-free JNS-Ti(salen)** gives much higher WCA value (84°) than **JNS-IL/Ti(salen)_{0.48}** (76°) (Fig. 4f vs. 4c). It suggests that the imidazolium-**IL** moiety also controls the surface wettability of **JNS-IL/Ti(salen)_x**. Notably, WCA values for all the catalytic nanosheets were lower than 90°. It suggests the relatively hydrophilic property and preferred oil-in-water (o/w) Pickering emulsions [37], which is favorable for aqueous catalysis.

3.2.5. Emulsifying capacity determination

Interfacial activity of **JNS-IL/Ti(salen)_x** was examined by testing their emulsifying capacity in a phenyl methyl sulfide/water system. Benefiting from the Janus characteristic, all **JNS-IL/Ti(salen)_x** give the highly dispersed Pickering emulsions, and the emulsions are stable for at least 24 h with no obvious change in physical appearance (Fig. 5A–C). While, emulsion stabilized by **HNS-IL/Ti**

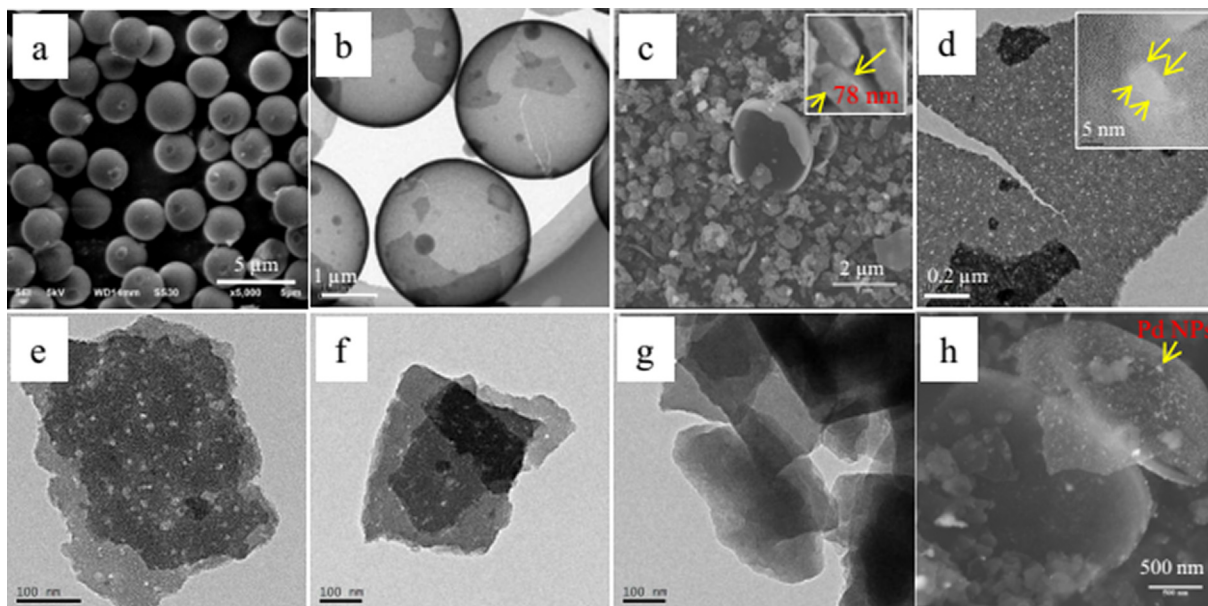


Fig. 2. SEM images of PS@mSiO₂ microspheres (a), JNS-IL/Ti(salen)_{0.48} (c) and Pd-labeled JNS (h), TEM images of JNS-IL/Ti(salen)_{0.48} before being crushed (b), JNS-IL/Ti(salen)_{0.48} (d, the inset is HRTEM image), JNS-Ti(salen) (e), HNS-IL/Ti(salen) (f), and ηJNS-IL/Ti(salen) (g).

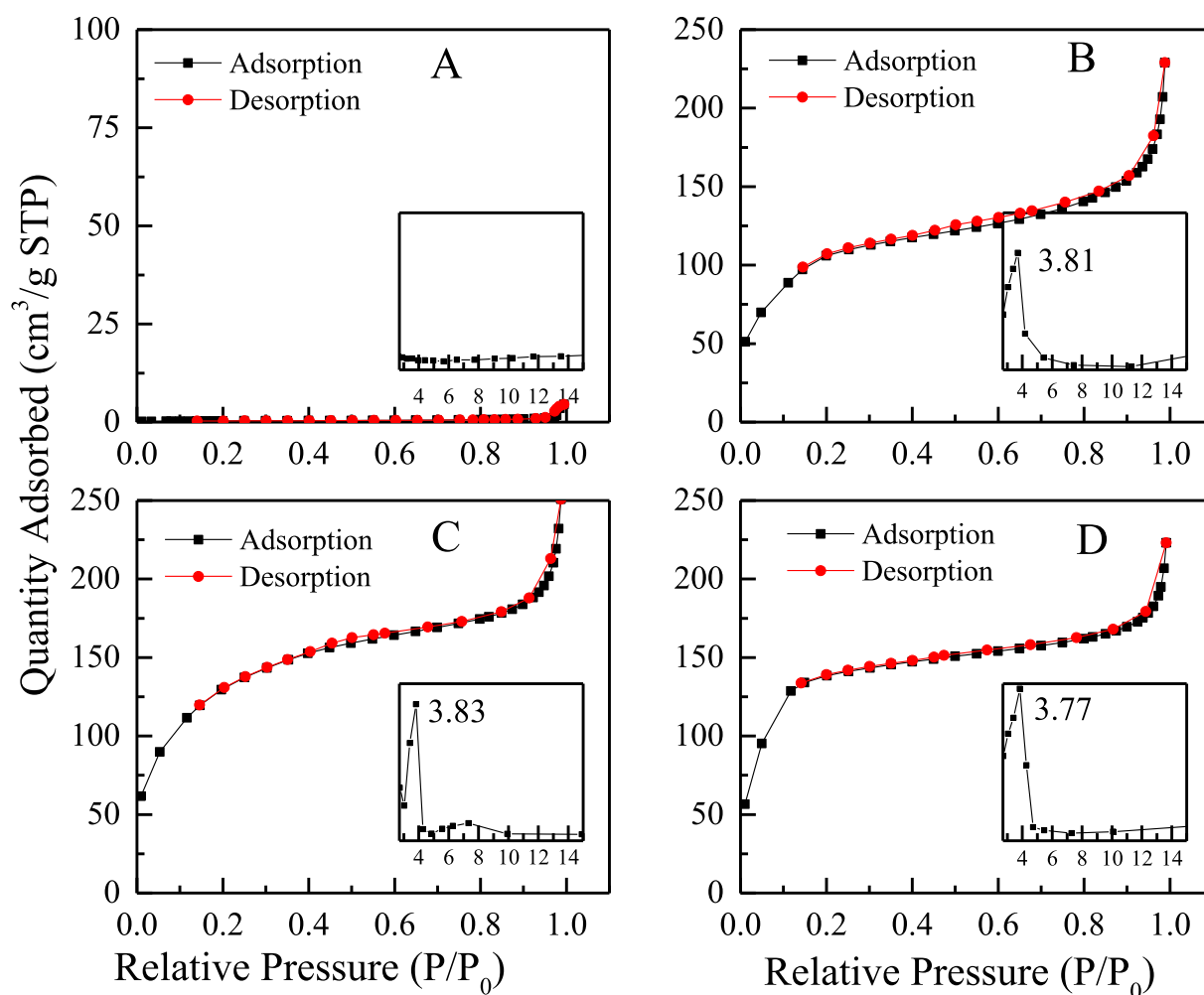


Fig. 3. Nitrogen adsorption–desorption isotherms and pore size distributions curves of ηJNS-IL/Ti(salen) (A), JNS-IL/Ti(salen)_{0.48} (B), pristine mesosilica nanosheet (C) and HNS-IL/Ti(salen) (D).

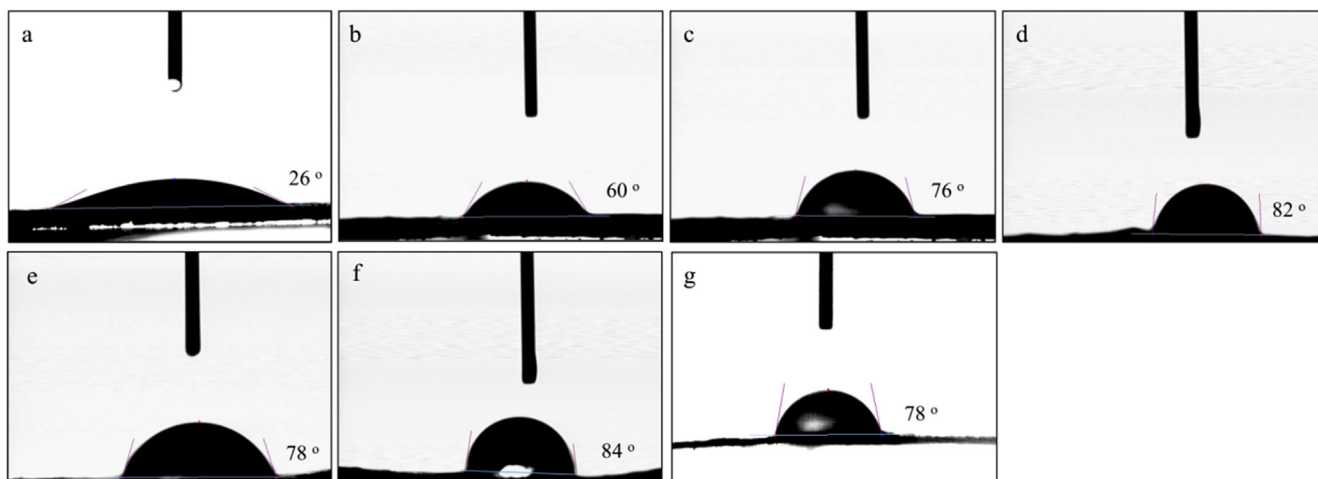


Fig. 4. WCA of pristine $m\text{SiO}_2$ nanosheet (a), $\text{JNS-IL/Ti(salen)}_{0.38}$ (b), $\text{JNS-IL/Ti(salen)}_{0.48}$ (c), $\text{JNS-IL/Ti(salen)}_{0.60}$ (d), HNS-IL/Ti(salen) (e), JNS-Ti(salen) (f), and $\eta\text{JNS-IL/Ti(salen)}$ (g).

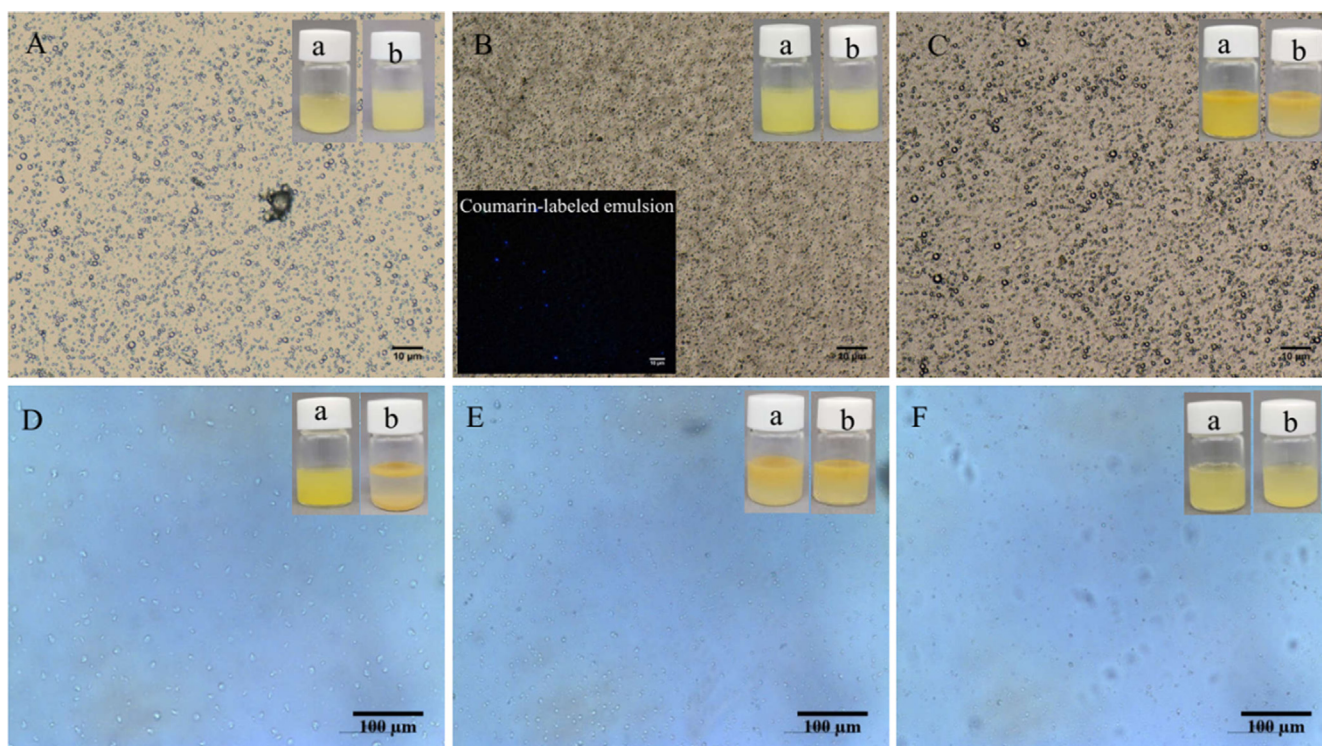


Fig. 5. Optical microscopy image of Pickering emulsions stabilized by $\text{JNS-IL/Ti(salen)}_{0.38}$ (A), $\text{JNS-IL/Ti(salen)}_{0.48}$ (B), $\text{JNS-IL/Ti(salen)}_{0.60}$ (C), HNS-IL/Ti(salen) (D), JNS-Ti(salen) (E), and $\eta\text{JNS-IL/Ti(salen)}$ (F). The inset shows the emulsion photos after standing for different times (a: 0 h; b: 24 h).

(salen) is unstable, and shows obvious phase separation after standing for 24 h (Fig. 5D). It is not surprised that the absorption energy of a Janus colloid at an oil/water interface is about 3 times than that of their counterpart uniform colloids [38], which thus stabilizes the Pickering emulsions. With the anisotropic surface wettability, JNS-Ti(salen) and $\eta\text{JNS-IL/Ti(salen)}$ also give stable Pickering emulsions with the droplet sizes in the range of 2–10 μm (Fig. 5E and 5F). To infer the emulsion type, coumarin dye was added to label the oil phase of $\text{JNS-IL/Ti(salen)}_{0.48}$ -stabilized Pickering emulsion. Blue oil droplets are clearly observed in the fluorescence microscope image (inserted in Fig. 5B), indicating that

the phenyl methyl sulfide is confined by surrounding water. This result demonstrates that the type of the resulting Pickering emulsion is o/w. Notably, the oil droplet size depends strongly upon the content of Ti(salen) group in the JNS emulsifier (Fig. 5A-C and Fig. S3). $\text{JNS-IL/Ti(salen)}_{0.48}$ gives the smallest emulsion droplets with diameter of ca. 1.0 μm (Fig. 5B). It is accompanied by a maximal interfacial contact area, which favors the interfacial mass transfer in interfacial catalysis. The stable sulfide/water Pickering emulsions, together with tunable interfacial contact area, makes $\text{JNS-IL/Ti(salen)}_x$ the desirable PIC for asymmetric sulfoxidation in water.

3.3. Catalytic performances

Since chiral sulfoxides are very important synthetic intermediates for widespread applications [39], the catalytic performances of **JNS-IL/Ti(salen)_x** were evaluated in the asymmetric oxidation of sulfides to enantiopure sulfoxides in water using aqueous H₂O₂ (30 wt%) as an oxidant. The results are summarized in Table 1.

Obviously, **JNS-IL/Ti(salen)_x** ($x = 0.38, 0.48, 0.60$) significantly accelerated asymmetric sulfoxidation with aqueous H₂O₂ in water through the formation of stable sulfide/water emulsion droplets (Table 1, entries 1–3). Kinetics study indicates that only 0.9 mol% of **JNS-IL/Ti(salen)_{0.48}** was sufficient to give almost quantitative yield (94%) of (*R*)-phenyl methyl sulfoxide with remarkable enantioselectivity (>99% ee) in water within 60 min (see Fig. S4 in ESI). In contrast, neat complex was inactive in the aqueous asymmetric sulfoxidation due to limited reaction interfacial area and high mass transport resistance, giving only 40% conversion of phenyl methyl sulfide with low chemoselectivity (66%) and ee value (81%) (Table 1, entry 4). There is no doubt that Pickering emulsions over **JNS-IL/Ti(salen)_x** should provide high oil/water interfacial areas and highly accessible reaction interfaces for the aqueous asymmetric oxidation of sulfides with H₂O₂. In fact, the interface-active mesoporous materials carry catalytically active Ti(salen) complexes to assemble at the oil/water interface, creating large oil (sulfide)-water interfacial area. A smaller size of emulsion droplets (**JNS-IL/Ti(salen)_{0.48}**) formed is more favorable for the transformation due to the larger oil/water interfacial areas for asymmetric catalysis (Table 1, entry 2 vs. entries 1 and 3). The formed emulsion effectively isolated sulfide from the surrounding aqueous environment, creating a concentrated environment for confined catalysis. Simultaneously, hydrophobic Ti(salen) side orients itself to oil (sulfide) phase at the oil/water interface, allowing for high local con-

centration of reactants around the active sites. Dense chiral salen Ti^{IV} complex confined in the oil phase may enforce a cooperative reaction pathway resulting in an enhanced reaction rate and higher selectivity [40]. Furthermore, H₂O which is the reduction product of H₂O₂ should rapidly diffuse out of oil droplet through the mesochannels, which further accelerated the aqueous asymmetric sulfoxidation. For these reasons, it is not surprised that the uniform **HNS-IL/Ti(salen)**, which gave less stable emulsions, showed much lower catalytic activity and selectivity under identical conditions (Table 1, entry 5).

Short and unhindered channels present on JNS should make the reaction interface highly accessible, and then improved the reaction rate of aqueous reactions. Indeed, nonporous **nJNS-IL/Ti(salen)** gave only 19% of conversion with lower chemoselectivity (86%) within 1 h, albeit with stable Pickering emulsion (Table 1, entry 6), and the catalytic efficiency had hardly increased even after 2 h (Table 1, entry 7 vs. 6). This is probably arisen from the nonporous structure of **nJNS-IL/Ti(salen)**, which cannot offer efficient passageway for the mass transfer of reactants on the interfaces. As a consequence, the **nJNS-IL/Ti(salen)** serves as physical barrier between the oil/water interfaces, making the reaction interfaces inaccessible. The results demonstrated the passageway effect of unhindered mesochannels in **JNS-IL/Ti(salen)_x**, which enables the rapid mass transfer of reagents inside and outside the emulsion droplets.

In addition to the fascinating mesoporous structure, highly accessible of reaction interface should also be related to the imidazolium-based IL spacer. Clearly, *IL*-free analog of **JNS-Ti(salen)** was far less active and selective than **JNS-IL/Ti(salen)_{0.48}** (Table 1, entry 8 vs. 2). Moderate conversion (69%) of phenyl methyl sulfide with only 87% chemoselectivity and 92% ee was obtained over **JNS-Ti(salen)** under identical conditions (Table 1,

Table 1
Results of asymmetric sulfoxidation over different chiral salen Ti^{IV} complexes in water.^a

Entry	Catalysts	R ₁	R ₂	T (h)	Conv. ^b (%)	Sel. ^b (%)	Ee. ^c (%)	TOF (h ⁻¹) ^d
1	JNS-IL/Ti(salen)_{0.38}	H	CH ₃	1	87	93	93 (<i>R</i>)	96.6
2	JNS-IL/Ti(salen)_{0.48}	H	CH ₃	1	98	96	99 (<i>R</i>)	109
3	JNS-IL/Ti(salen)_{0.60}	H	CH ₃	1	83	82	94 (<i>R</i>)	92.2
4	neat complex	H	CH ₃	1	40	66	81 (<i>R</i>)	44.4
5	HNS-IL/Ti(salen)_{0.48}	H	CH ₃	1	65	87	94 (<i>R</i>)	72.2
6	nJNS-IL/Ti(salen)_{0.48}	H	CH ₃	1	19	86	99 (<i>R</i>)	21.1
7	nJNS-IL/Ti(salen)_{0.48}	H	CH ₃	2	21	89	99 (<i>R</i>)	11.7
8	JNS-Ti(salen)_{0.48}	H	CH ₃	1	69	87	92 (<i>R</i>)	76.7
9	HO-SiO ₂ - <i>IL</i> -Ti(salen) _{0.07}	H	CH ₃	1	99	97	98 (<i>R</i>)	79.2 ^e
10	JNS-IL/Ti(salen)_{0.48}	H	C ₂ H ₅	1	93	95	99 (<i>R</i>)	103
11	neat complex	H	C ₂ H ₅	1	23	70	90 (<i>R</i>)	25.6
12	JNS-IL/Ti(salen)_{0.48}	H	<i>n</i> -C ₄ H ₉	1.5	97	97	94 (<i>R</i>)	71.9
13	neat complex	H	<i>n</i> -C ₄ H ₉	1.5	25	66	90 (<i>R</i>)	18.5
14	JNS-IL/Ti(salen)_{0.48}	H	<i>n</i> -C ₆ H ₁₃	2	90	99	92 (<i>R</i>)	50.0
15	neat complex	H	<i>n</i> -C ₆ H ₁₃	2	13	99	79 (<i>R</i>)	7.8
16	JNS-IL/Ti(salen)_{0.48}	2-OCH ₃	CH ₃	2	95	97	99 (<i>R</i>)	51.1
17	neat complex	2-OCH ₃	CH ₃	2	37	72	96 (<i>R</i>)	20.6
18	JNS-IL/Ti(salen)_{0.48}	4-OCH ₃	CH ₃	1	92	98	88 (<i>R</i>)	94.4
19	neat complex	4-OCH ₃	CH ₃	1	22	71	76 (<i>R</i>)	24.4
20	JNS-IL/Ti(salen)_{0.48}	4-Br	CH ₃	1	21	90	99 (<i>R</i>)	18.9
21	neat complex	4-Br	CH ₃	1	31	66	92 (<i>R</i>)	34.4

^a Catalyst (0.9 mol% of substrate, based on titanium content), substrate (1.0 mmol), H₂O₂ (1.2 mmol, added in 15 min), H₂O (1.0 mL), 60 min, 25 °C.

^b Determined by GC.

^c Determined by HPLC (Daicel chiralpak AD column).

^d Turn over frequency (TOF) is calculated by [product]/[catalyst] × time (h⁻¹).

^e HO-SiO₂-*IL*-Ti(salen)_{0.07} (1.25 mol% of substrate, based on titanium content), phenyl methyl sulfide (1.0 mmol), H₂O₂ (1.2 mmol, added in 15 min), H₂O (1.0 mL), 60 min, 25 °C [Ref. [28]].

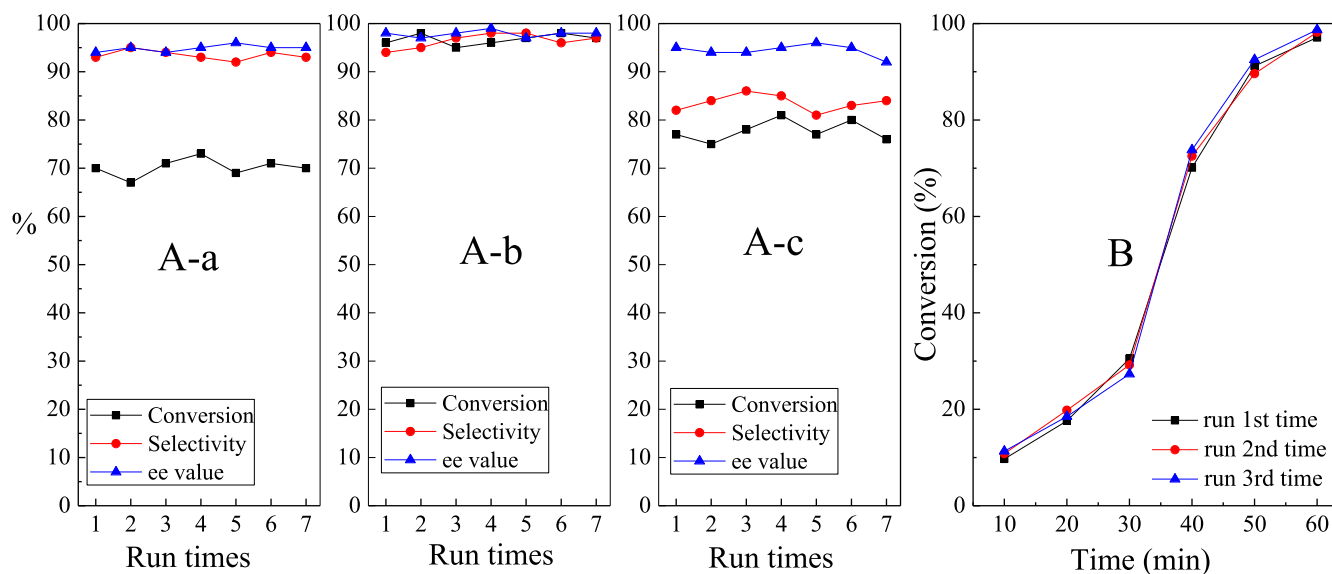


Fig. 6. (A) Reuse of **JNS-IL/Ti(salen)_{0.38}** (a), **JNS-IL/Ti(salen)_{0.48}** (b) and **JNS-IL/Ti(salen)_{0.60}** (c) in asymmetric sulfoxidation of phenyl methyl sulfide in water, (B) kinetic curves of the consecutive experimental runs 1–3 over **JNS-IL/Ti(salen)_{0.48}**.

entry 8). In fact, the IL moiety with unique solvent power [41] was assembled at the oil/water interface along with Ti(salen) units. It made the reaction interface more compatible with organic sulfides and aqueous H₂O₂, increasing the concentrations of reactants at the interface. Furthermore, the imidazolium-based IL linker places the chiral salen Ti^{IV} complex away from the silica sheets, enabling all bulk active sites to adapt their preferential conformation for favorable cooperative action. High polarity and ionic properties of ILs also had a positive effect on stabilizing the formed active metallosalen intermediate, which in turn improves the catalytic efficiency of **JNS-IL/Ti(salen)_x** [42].

Benefiting from the high oil/water interfacial areas together with highly accessible reaction interfaces, **JNS-IL/Ti(salen)_{0.48}** was also efficient for a wide range of aryl alkyl sulfides, such as phenyl ethyl sulfide, phenyl *n*-butyl sulfide, phenyl *n*-hexyl sulfide, *p*-methoxyphenyl methyl sulfide, and *o*-methoxyphenyl methyl sulfide. Almost quantitative yields of the corresponding chiral sulfoxides (92–98%) were obtained over an extremely low amount of **JNS-IL/Ti(salen)_{0.48}** (0.9 mol%) in water (Table 1, entries 10, 12, 14, 16 and 18). In particular, in the case of phenyl *n*-butyl sulfide, the yield of chiral phenyl *n*-butyl sulfoxide over **JNS-IL/Ti(salen)_{0.48}** increased even up to 7 times as compared with that of neat complex (Table 1, entry 14 vs. 15). Despite still being aryl alkyl sulfide, *p*-bromophenyl methyl sulfide underwent a slower oxidation (21% of conversion) over **JNS-IL/Ti(salen)_{0.48}** in water, although the chemo- (90%) and enantioselectivity (99%) were encouraging (Table 1, entry 20). It is probably due to that, unlike the other liquid sulfides, *p*-bromophenyl methyl sulfide is solid and unfavorable for the formation of oil/water emulsions for efficient interfacial catalysis. The observations provided further evidence for the Pickering interfacial catalysis of asymmetric sulfoxidation in water.

Notably, the mesoporous **JNS-IL/Ti(salen)_{0.48}** was even more efficient than our reported Janus HO-SiO₂-IL-Ti(salen)_{0.07} nanospheres, although the latter also provided a highly accessible reaction interface. As shown in Table 1, **JNS-IL/Ti(salen)_{0.48}** afforded TOF value of 109 h⁻¹, which is 1.4 times higher than that of HO-SiO₂-IL-Ti(salen)_{0.07} (79.2 h⁻¹) (Table 1, entry 2 vs. 9). Higher efficiency of **JNS-IL/Ti(salen)_{0.48}** should benefit from the two-dimensional nanosheets structure which restrict the rotation of

Janus platelets at the oil/water interface to a great degree, thus making the emulsion relatively more stable [14,15]. Such a two-dimensional structure also extremely shortens the diffusion distance for sulfide and H₂O₂ at the oil/water interface, enhancing the mass transfer of reactants on the interfaces [16–19]. Furthermore, the active sites on sheet-shaped materials are easily exposed in comparison to those of the sphere-shaped particles, leading to the large surface areas, which would be favorable for the catalysis process to some degree [43,44].

Apart from the observed acceleration effect, another salient feature of the **JNS-IL/Ti(salen)_x** is its facile recovery. After reaction, the novel catalysts could be quantitatively recovered from the aqueous system by simple centrifugation, and re-formed the stable Pickering emulsion for the recycle experiment. Fig. 6A shows the reusability of **JNS-IL/Ti(salen)_x** in the asymmetric oxidation of phenyl methyl sulfide in water. To our delight, all **JNS-IL/Ti(salen)_x** catalysts could be reused at least ten times without significant loss in activity and selectivity. ICP-OES analysis gave titanium content in recovered **JNS-IL/Ti(salen)_x** of 0.376, 0.473, and 0.597 mmol g⁻¹ for *x* = 0.38, 0.48, and 0.60, respectively, which was almost identical to that of the corresponding fresh one. Indeed, negligible amount of titanium was detected in the supernatant according to ICP-OES analysis, which revealed the negligible leaching loss of titanium species during the reaction. More importantly, all **JNS-IL/Ti(salen)_x** were stable to oxidative decomposition during H₂O₂-based oxidation, as evident from the FT-IR spectra of typical **JNS-IL/Ti(salen)_{0.48}** (Fig. 1b vs. 1b'). Kinetics study provided the other substantial proof for the stability of **JNS-IL/Ti(salen)_x**, based on the fact that no significant change in the apparent rate constant occurred in the consecutive experimental runs 1–3 over typical **JNS-IL/Ti(salen)_{0.48}** (Fig. 6B). The excellent stability of catalysts should arise from the shielding of the chiral salen Ti^{IV} complex in oil droplets, which potentially protected the Ti(salen) complex from oxidative decomposition by aqueous H₂O₂ [45]. Furthermore, the imidazolium IL moiety assembled at the oil/water interface along with Ti(salen) units should also have a positive effect on stabilizing the complex [42]. The facile recovery together with the perfect stability makes **JNS-IL/Ti(salen)_x** highly promising in sustainable industrial applications.

4. Conclusions

A novel IL-functionalized amphiphilic Janus mesosilica nanosheet which contains Ti(salen) complex on one side has been prepared *via* simply crushing hollow mesosilica microspheres with two distinct surfaces. The two-dimensional porous Janus structure together with the compatible IL modifier endowed the JNS catalysts with excellent interfacial activity as well as highly accessible reaction interface for reactants. As a consequence, the IL-functionalized JNS materials induced an efficient Pickering interfacial catalysis approach for asymmetric sulfoxidation in water using H₂O₂ as an oxidant, leading to significant rate acceleration and remarkable high selectivity over a wide range of aryl alkyl sulfides. In addition, they can be facilely recovered from the aqueous system for efficient reuse by simple centrifugation. The novel catalytic system offers several advantages, such as operational simplicity, mild reaction conditions, high efficiency, effective separation of final products, and facile reuse of catalyst. All these advantages make it a benign protocol from the sustainability point of view, and inspired us to design the other advanced interface-active catalyst for a wide range of sustainable industrial applications.

Declaration of Competing Interest

The authors declare that they have no known competing financial interests or personal relationships that could have appeared to influence the work reported in this paper.

Acknowledgements

The authors are grateful for the financial support provided by the National Natural Science Foundation of China (21676078), the Scientific Research Fund of Hunan Provincial Education Department (19A323), and the Key Laboratory of the Assembly and Application of Organic Functional Molecules of Hunan Province. We also thank Dr. Jiajun Wang and Mingjie Zhang for their helpful discussions.

Appendix A. Supplementary material

Supplementary data to this article can be found online at <https://doi.org/10.1016/j.jcat.2021.01.022>.

References

- [1] W. Guo, X. Liu, Y. Liu, C. Li, ACS Catal. 8 (2018) 328–341, <https://doi.org/10.1021/acscatal.7b02118>.
- [2] E. Rytter, Ø. Borge, N. E. Tsakoumis, A. Holmena, J. Catal. 365 (2018) 334–343, <https://doi.org/10.1016/j.jcat.2018.07.003>.
- [3] A.P. Gerola, E.H. Werlind, Y.S. Gomes, L.A. Giusti, G. Luis, R.A. Nome, A.J. Kirdey, H.D. Fiedler, F. Nome, ACS Catal. 7 (2017) 2230–2239, <https://doi.org/10.1021/acscatal.7b00097>.
- [4] H. Heinz, C. Pramanik, O. Heinz, Y. Ding, R.K. Mishra, D. Marchon, R.J. Flatt, I.E. Lopus, J. Llop, S. Moya, R.F. Ziolo, Surf. Sci. Rep. 72 (2017) 1–58, <https://doi.org/10.1016/j.surfrep.2017.02.001>.
- [5] Y. Hao, X. Jiao, H. Zou, H. Yang, J. Liu, J. Mater. Chem. A 5 (2017) 16162–16170, <https://doi.org/10.1039/C6TA11124F>.
- [6] J. Cho, J. Cho, H. Kim, M. Lim, H. Jo, H.C. Kim, S.J. Min, H. Rhee, J.W. Kim, Green Chem. 20 (2018) 2840–2844, <https://doi.org/10.1039/C8GC00282G>.
- [7] L. Wei, M. Zhang, X. Zhang, H. Xin, H. Yang, ACS Sustain. Chem. Eng. 4 (2016) 6838–6843, <https://doi.org/10.1021/acssuschemeng.6b01776>.
- [8] J. Tang, Q. Zhang, K. Hu, S. Cao, S. Zhang, J. Wang, J. Catal. 368 (2018) 190–196, <https://doi.org/10.1016/j.jcat.2018.10.003>.
- [9] X. Zhang, Y. Hou, R. Etlelaie, R.G.M. Zhang, Y. Zhang, H. Yang, J. Am. Chem. Soc. 141 (2019) 5220–5230, <https://doi.org/10.1021/jacs.8b11860>.
- [10] M. Tang, X. Wang, F. Wu, Y. Liu, S. Zhang, X. Pang, X. Li, H. Qiu, Carbon 71 (2014) 238–248, <https://doi.org/10.1016/j.carbon.2014.01.034>.
- [11] Y. Liu, J. Hu, X. Yu, X. Xu, Y. Gao, H. Li, F. Liang, J. Colloid Interf. Sci. 490 (2017) 357–364, <https://doi.org/10.1016/j.jcis.2016.11.053>.
- [12] J. Dai, H. Zou, Z. Shi, H. Yang, R. Wang, Z. Zhang, S. Qiu, ACS Appl. Mater. Interfaces 10 (2018) 33474–33483, <https://doi.org/10.1021/acsami.8b11888>.
- [13] T. Zhao, X. Zhu, C. Hung, P. Wang, A. Elzatahry, A.A. Al-Khalaf, W.N. Hozzein, F. Zhang, X. Li, D. Zhao, J. Am. Chem. Soc. 140 (2018) 10009–10015, <https://doi.org/10.1021/jacs.8b06127>.
- [14] R. Deng, F. Liang, P. Zhou, C. Zhang, X. Qu, Q. Wang, J. Li, J. Zhu, Z. Yang, Adv. Mater. 26 (2014) 4469–4472, <https://doi.org/10.1002/adma.201305849>.
- [15] T. Yin, Z. Yang, F. Zhang, M. Lin, J. Zhang, Z. Dong, J. Colloid Interf. Sci. 583 (2021) 214–221, <https://doi.org/10.1016/j.jcis.2020.09.026>.
- [16] Al C. de Leon, B.J. Rodier, Q. Luo, C.M. Hemmingsen, P. Wei, K. Abbasi, R. Advincula, E.B. Pentzer, ACS Nano 11 (2017) 7483–7493, <https://doi.org/10.1021/acsnano.7b04020>.
- [17] Y. Lin, M.R. Thomas, A. Gelmi, V. Leonardo, E.T. Pashuck, S.A. Maynard, Y. Wang, M.M. Stevens, J. Am. Chem. Soc. 139 (2017) 13592–13595, <https://doi.org/10.1021/jacs.7b06591>.
- [18] H. Nie, X. Liang, A. He, Macromolecules 51 (2018) 2615–2620, <https://doi.org/10.1021/acs.macromol.8b00039>.
- [19] S. Yan, H. Zou, S. Chen, N. Xue, H. Yang, Chem. Commun. 54 (2018) 10455–10458, <https://doi.org/10.1039/c8cc05967e>.
- [20] H. Zhang, Y. Zhang, C. Li, J. Catal. 238 (2006) 369–381, <https://doi.org/10.1016/j.jcat.2005.12.023>.
- [21] J. Kim, B. Song, G. Hwang, Y. Bang, Y. Yun, J. Catal. 373 (2019) 306–313, <https://doi.org/10.1016/j.jcat.2019.04.006>.
- [22] R.I. Kureshy, T. Roy, N.H. Khan, S.H.R. Abdi, A. Sadukhan, H.C. Bajaj, J. Catal. 286 (2012) 41–50, <https://doi.org/10.1016/j.jcat.2011.10.011>.
- [23] Z. Tang, W. Wang, Y. Pi, J. Wang, C. Li, R. Tan, ACS Sus. Chem. Eng. 7 (2019) 17967–17978, <https://doi.org/10.1021/acssuschemeng.9b04712>.
- [24] N. Yan, C. Chen, D. Li, Y. Hu, J. Environ. Chem. Eng. 11 (2019) 10967–10974, <https://doi.org/10.1016/j.jece.2020.103953>.
- [25] R. Zhao, X. Yu, D. Sun, L. Huang, F. Liang, Z. Liu, ACS Appl. Nano Mater. 2 (2019) 2127–2132, <https://doi.org/10.1021/acsnano.9b00090>.
- [26] S. Colonna, R. Fornasier, Synthesis 80 (1975) 531–532, <https://doi.org/10.1055/s-1975-23836>.
- [27] C. Lv, D. Xu, S. Wang, C. Miao, C. Xia, W. Sun, Catal. Commun. 12 (2011) 1242–1245, <https://doi.org/10.1016/j.catcom.2011.04.022>.
- [28] M. Zhang, Z. Tang, W. Fu, W. Wang, R. Tan, D. Yin, Chem. Commun. 55 (2019) 592–595, <https://doi.org/10.1039/C8CC08292H>.
- [29] W. Ming, J. Zhao, X. Lu, C. Wang, S. Fu, Macromolecules 29 (1996) 7678–7682, <https://doi.org/10.1021/ma951134d>.
- [30] Z. Deng, M. Chen, S. Zhou, B. You, L. Wu, Langmuir 22 (2006) 6403–6407, <https://doi.org/10.1021/la060944n>.
- [31] W. Peng, P. Hao, J. Luo, B. Peng, X. Han, H. Liu, Ind. Eng. Chem. Res. 59 (2020) 4272–4280, <https://doi.org/10.1021/acs.iecr.9b06097>.
- [32] G. Zhao, B. Hong, B. Bao, S. Zhao, M. Pera-Titus, J. Phys. Chem. C 123 (2019) 12818–12826, <https://doi.org/10.1021/acs.jpcc.9b01876>.
- [33] L. Yu, Y. Zhang, L. Xu, Q. Liu, B. Borjigin, D. Hou, J. Xiang, J. Wang, Sep. Purif. Technol. 250 (2020) 117245, <https://doi.org/10.1016/j.seppur.2020.117245>.
- [34] Y. Feng, L. Li, X. Wang, J. Yang, T. Qiu, Energ. Convers. Manage. 153 (2017) 649–658, <https://doi.org/10.1016/j.enconman.2017.10.018>.
- [35] H. Suo, L. Xu, C. Xu, X. Qiu, H. Huang, Y. Hu, J. Colloid Interf. Sci. 553 (2019) 494–502, <https://doi.org/10.1016/j.jcis.2019.06.049>.
- [36] H. Zou, R. Wang, X. Li, X. Wang, S. Zeng, S. Ding, L. Li, Z. Zhang, S. Qiu, J. Mater. Chem. A 2 (2014) 12403–12412, <https://doi.org/10.1039/C4TA01943A>.
- [37] M. Momenni, H. Saghafian, F. Golestaran, A. Khanahmadi, Appl. Surf. Sci. 392 (2017) 80–87, <https://doi.org/10.1016/j.apsusc.2016.08.165>.
- [38] F. Liang, B. Liu, Z. Cao, Z. Yang, Langmuir 34 (2018) 4123–4131, <https://doi.org/10.1021/acs.langmuir.7b02308>.
- [39] J. Han, V.A. Soloshonok, K.D. Klika, J. Drabowicz, A. Wzorek, Chem. Soc. Rev. 47 (2018) 1307–1350, <https://doi.org/10.1039/C6CS00703A>.
- [40] C. Freire, M. Nunes, C. Pereira, D.M. Fernandes, A.F. Peixoto, M. Rocha, Coord. Chem. Rev. 394 (2019) 104–134, <https://doi.org/10.1016/j.ccr.2019.05.014>.
- [41] B. Karimi, M. Tavakolian, M. Akbari, F. Mansouri, ChemCatChem 10 (2018) 3173–3205, <https://doi.org/10.1002/cctc.201701919>.
- [42] N. Vucetic, P. Virtanen, A. Nuri, I. Mattsson, A. Aho, J. Mikkola, T. Salmi, J. Catal. 371 (2019) 35–46, <https://doi.org/10.1016/j.jcat.2019.01.029>.
- [43] F. Liang, K. Shen, X. Qu, C. Zhang, Q. Wang, J. Li, J. Liu, Z. Yang, Angew. Chem. Int. Edit. 123 (2011) 2379–2382, <https://doi.org/10.1002/ange.201007519>.
- [44] S. Zhang, Q. Deng, H. Shangguan, C. Zhang, J. Shi, F. Huang, B. Tang, ACS Appl. Mater. Interfaces 12 (2020) 12227–12237, <https://doi.org/10.1021/acsnano.9b18735>.
- [45] A. Lu, R.K. O'Reilly, Curr. Opin. Biotech. 24 (2013) 639–645, <https://doi.org/10.1016/j.copbio.2012.11.013>.